Received: 22 December 2020 | Revised: 10 May 2021 | Accepted: 6 June 2021

DOI: 10.1002/nag.3251

RESEARCH ARTICLE

WILEY

Three-dimensional ridge collapse mechanism for narrow soil slopes

Radoslaw L. Michalowski[1] | **Dowon Park**[2]

[1] Deparment of Civil and Environmental Engineering, University of Michigan, Ann Arbor, Michigan, USA

[2] Department of Civil Engineering, University of Seoul, Seoul, South Korea

Correspondence
Radoslaw L. Michalowski, Department of Civil and Environmental Engineering, University of Michigan, 2028 G.G. Brown Bldg., 2350 Hayward, Ann Arbor, MI 48109, USA.
Email: rlmich@umich.edu

Abstract

Three-dimensional analysis of stability is carried out for slopes with the failure mechanism confined to a narrow space. A curvilinear cone failure surface is modified by removing a slice from its central portion, to make the failure mechanism fit in the narrow space. The resulting surface is no longer smooth, and it is referred to as the *ridge mechanism* for a distinct ridge in the failure surface. The analysis of narrow slopes based on the ridge mechanism appears to yield lower stability factors than the mechanisms used in geotechnical engineering thus far. Kinematic limit analysis utilized in calculations provides an upper bound to the true stability factor solution, hence the newly proposed mechanism delivers a more accurate solution.

KEYWORDS

landslides, limit analysis, plasticity analysis, ridge failure surface, slope stability

1 | INTRODUCTION AND PROBLEM STUDIED

Assessment of safety of earth slopes has a rich literature, particularly for wide slopes where the failure can be approximated with a two-dimensional collapse mechanism. This paper relates to narrow slopes, which call for a three-dimensional analysis. In the last decade, a mechanism suggested by Michalowski and Drescher[1,2] became widely accepted in limit analysis of slopes. This mechanism was postulated based on the kinematic admissibility of a rotational motion of the soil block in soil governed by the Mohr-Coulomb failure criterion and the normality plastic flow rule. The failure surface in this mechanism was patterned after the surface used in three-dimensional stability analysis of rectangular footings.[3] Even though the rotational motion is considered as a slope incipient failure mechanism, whereas the translational mechanism governs the footing collapse,[3] the failure surfaces have the same characteristics. The shape of this failure surface resembles a curvilinear cone, and it is of the same type as the one derived by means of variational calculus by Leshchinsky et al.,[4,5] though the latter does not provide the same geometric flexibility, as discussed elsewhere.[6] Over the last decades, there were a number of attempts at 3D limit analyses of slopes in pressure-dependent soils besides those already mentioned.[7–9] Observation of results indicates that the rotational mechanisms are typically more efficient (yield a more accurate bound to a safety measure) than the translational mechanisms are. Therefore, a rotational mechanism for narrow slopes is pursued in this paper.

While the method used in this paper includes the kinematic approach of limit analysis, other methods have been used equally often in the subject of three-dimensional safety assessment of slopes. For example, more recent applications of the finite element method can be found in Hicks and Li[10] or Cremonesi et al.,[11] whereas the FEM approach in limit analysis is used in Camargo et al.[12] A more traditional though recent application of a limit equilibrium method can be found in Tun et al.[13]

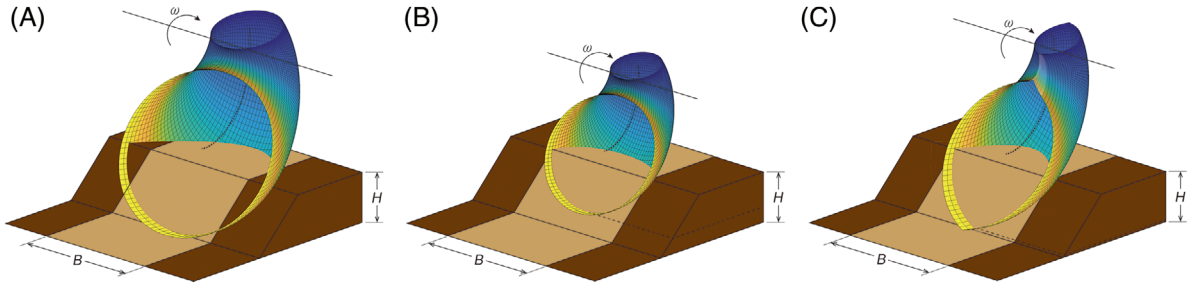

FIGURE 1 View of the failure surface intersecting a slope with width constraint B: (A) failure surface passing through the toe, but exceeding the slope width constraint, (B) failure surface matching the slope width, but passing through the slope face (face failure), and (c) ridge failure surface matching width B

It was pointed out throughout the literature that if the slope is very narrow (width smaller than height), then a toe mechanism with the curved cone failure surface may not be accommodated by this narrow space. This is illustrated in Figure 1A, where the size of the slope is limited to the light-colored portion with width B, whereas the dark sections on either side are to simulate the geometric constraints, for example, rock outcrop. A common procedure is then to scale down the surface with respect to the slope, so that it fits in the space between the constraints. This, however, will no longer be a toe mechanism; rather, the surface will intersect the face of the slope as illustrated in Figure 1B. This type of failure pattern is referred to as a *face failure*. An approach investigated in this paper is based on a different concept. This study is motivated by an observation that the traditional *face failure* is a common mechanism used in slope analyses, but scaled to a height smaller than the actual slope height, so that it can be accommodated in a slope with a stringent width constraint. There is no effort in such analyses to make the mechanisms more accurate in assessing the slope safety, but only to make them kinematically admissible, that is, consistent with the plastic flow rule. The authors do not have a database with slopes failed in narrow spaces, and the study is based on a purely theoretical effort of constructing a new mechanism that appears to yield better assessment of the slope safety measures.

In order to assure that the stability analysis solution tends to a 2D solution in the absence of a constraint on the slope width, a prismatic insert is placed in the center of the mechanism.[1] For a very narrow slope, it is now suggested that a slice of the horn-shape failing block be removed from the block's central section, so that the combined width of the remaining portions matches the constraining width B. This is illustrated in Figure 1C. The failure surface is no longer smooth, and it has a distinct *ridge* coinciding with the symmetry plane. This failure mechanism will be referred to as the *ridge mechanism*. A similar approach was used recently in an analysis of slopes in intact rock governed by the Hoek-Brown failure criterion.[14] The concept of the collapse mechanism is very similar to that in the recent paper,[14] but the form of the failure surface and its mathematical description is different as the kinematic admissibility in the two cases is governed by the plastic flow rule associated with strength envelopes of considerably different shape. This paper attempts to determine whether the ridge mechanism can yield a more accurate assessment of the slope safety than the mechanisms, which utilize the smooth failure surfaces in soil slope engineering.

2 | APPLICATION OF LIMIT ANALYSIS IN STABILITY ASSESSMENT

2.1 | Kinematic limit analysis

The method used in this paper is the kinematic approach of limit analysis. The premise upon which the method is developed is a material model with convexity of the failure criterion and the normality of the plastic flow rule. These assumptions allow one to prove that the rate of dissipated work during incipient failure in any kinematically admissible mechanism is not smaller than the work rate of true external forces in that mechanism. For slopes loaded with self-weight alone, and failure occurring only along failure surfaces L, this theorem can be written as

$$\int_L T_i[v]_i dL \geq \int_V X_i v_i dV \tag{1}$$

where T_i and $[v]_i$ are the stress vector and velocity discontinuity vector on failure surfaces L, and X_i and v_i are the gravity force vector acting in mechanism volume V and the velocity vector, respectively.

The left-hand side of the theorem in Equation (1) represents the rate of dissipated work in an incipient failure process, whereas the right-hand side is the work rate of gravity forces. Finding both rates in an admissible collapse mechanism makes it possible to arrive at a rigorous bound to the true solution for a selected measure of slope safety.

2.2 | Measures of slope safety

Any slope of given inclination can be characterized by a dimensionless group $\gamma H/c$, where γ, H and c are the unit weight of the soil, slope height, and soil cohesion, respectively. Such a characterization presumes that the strength of the soil is defined by the Mohr-Coulomb criterion. For every slope, there is a limiting value of this dimensionless group; if this limiting (or critical) value is reached, the collapse of the slope is imminent. This critical value of dimensional group $\gamma H/c$ is referred to as *stability factor*[15] N_f

$$N_f = \left(\frac{\gamma H}{c}\right)_{crit} \tag{2}$$

The difference between dimensionless group $\gamma H/c$ and its critical value N_f is indicative of the margin of safety. For an undrained process of failure, the stability factor is defined as

$$N_f = \left(\frac{\gamma H}{s_u}\right)_{crit} \tag{3}$$

where s_u is the undrained shear strength of the soil. The kinematic approach of limit analysis used in this paper yields an upper bound to the stability factor.

A reciprocal of the stability factor is often used in the assessment of safety, as it allows for presentation of a wider range of the results without resorting to the log scale. It is referred to as *stability number* N_n and can be written as

$$N_n = \left(\frac{c}{\gamma H}\right)_{crit} \tag{4}$$

The stability factor and the stability number contain essentially the same information, although the safety of the slope decreases with an increase in the dimensionless group $\gamma H/c$, whereas the slope safety increases with an increase of group $c/\gamma H$. The kinematic approach of limit analysis yields a lower bound to the stability number.

A more traditional slope safety measure, but also more intuitive, is *factor of safety* F. It is defined as the ratio of the shear strength of soil τ to the demand on the shear strength τ_d needed for stability

$$F = \frac{\tau}{\tau_d} \tag{5}$$

The kinematic approach yields the upper bound to the factor of safety. All three measures will be considered in this paper.

3 | THREE-DIMENSIONAL RIDGE FAILURE MECHANISM

3.1 | Mechanism geometry

A toe failure mechanism, patterned after Michalowski and Drescher,[1] is shown in Figure 2A, whereas the transformation of this mechanism into a ridge mechanism is illustrated in Figure 2B. The failure block rotating about an axis passing through point O has a horn-like shape (a curved cone), with lower and upper contours described by the following two

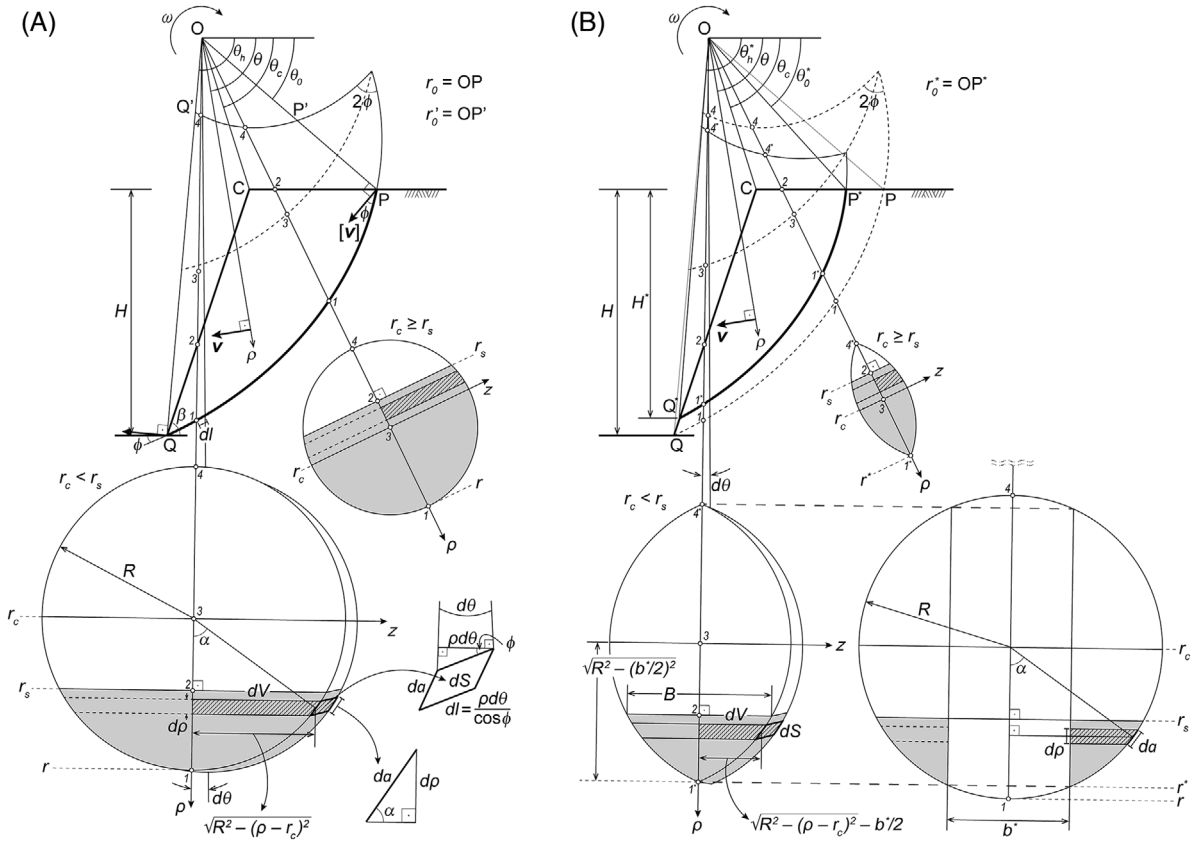

FIGURE 2 Cross-section of the failure mechanism: (A) classical toe mechanism,[1] and (B) ridge mechanism

log-spirals

$$r = r_0 e^{(\theta-\theta_0)\tan\phi} \tag{6}$$

$$r' = r'_0 e^{-(\theta-\theta_0)\tan\phi} \tag{7}$$

with r_0 and r'_0 equal to OP and OP' (Figure 2A), respectively; θ_0 is the angular coordinate of points P and P', and ϕ is the internal friction angle of the soil. The radii in Equations (6) and (7) are quite different from those in intact rocks considered in Park and Michalowski.[14] This is the consequence of kinematic admissibility governed by the normality flow rule used with different failure criteria in the two cases. A cross-section of the rotating block with any plane perpendicular to the plane of the figure and passing through point O forms a circle of radius R

$$R(\theta) = \frac{r(\theta) - r'(\theta)}{2} \tag{8}$$

and the center of the circular cross-section is located at distance r_c from point O

$$r_c(\theta) = \frac{r(\theta) + r'(\theta)}{2} \tag{9}$$

If a toe mechanism so constructed violates width constraint B (as in Figure 1A), then it is possible to transform this mechanism into a ridge mechanism by extracting a vertical slice of the rotating block from its middle portion, as illustrated in Figures 1C and 2B. The width of the slice to be extracted, b^*, can be found as the larger value calculated from the two

following expressions

$$\begin{aligned} b^* &= 2 \cdot \max(R) - B, && r_c \geq r_s \\ b^* &= 2 \max\left[\sqrt{R^2 - (r_s - r_c)^2}\right] - B, && r_c < r_s \end{aligned} \tag{10}$$

where B is the width constraint on the size of the mechanism, r_c is expressed in Equation (9), and r_s describes the slope contour in the polar coordinate system and is given in the Appendix (Equation A1). After removing the vertical slice of width b^* from the central portion of the block, the two remaining parts combined into one block form a surface with a discontinuous derivative along the symmetry plane as indicated on two cross-sections in Figure 2B. The block now fits exactly into width B. Contrary to line PQ, the ridge in the surface, line P^*Q^*, is no longer a log-spiral, and its radial coordinate r^* is described in the following expression

$$r^*(\theta) = r_c(\theta) + \sqrt{R^2(\theta) - \left(\frac{b^*}{2}\right)^2}, \qquad \theta_0^* \leq \theta < \theta_h^* \tag{11}$$

where θ_0^* and θ_h^* are the angular coordinates of point P^* on the top surface and point Q^* on the slope just above the toe, respectively. The failure surface in a ridge mechanism so constructed does not pass through the toe (i.e., $\theta_h^* < \theta_h$). Both θ_0^* and θ_h^* can be found from implicit equations (solved iteratively), which make use of the condition that both P^* and Q^* are located on the slope contour defined by radius r_s (Equation A1)

$$r_c(\theta_0^*) + \sqrt{R^2(\theta_0^*) - \left(\frac{b^*}{2}\right)^2} = r_s(\theta_0^*) \tag{12}$$

$$r_c(\theta_h^*) + \sqrt{R^2(\theta_h^*) - \left(\frac{b^*}{2}\right)^2} = r_s(\theta_h^*) \tag{13}$$

3.2 | Rates of work dissipation and gravity work in the ridge mechanism

Rigorous bounds to specific stability or safety measures are calculated from the balance equation, in which the two terms in Equation (1), rate of dissipation D and gravity work rate W_γ, are taken as equal to one another

$$D = W_\gamma \tag{14}$$

Rate of work dissipation d per unit area of the failure surface is[16]

$$d = c[v]\cos\phi \tag{15}$$

where $[v]$ is the magnitude of the velocity discontinuity vector $[\mathbf{v}]$ on the failure surface. Introducing infinitesimal area of failure surface dS (Figure 2)

$$dS = dl\, da = \frac{\rho}{\cos\phi} \frac{R}{\sqrt{R^2 - (\rho - r_c)^2}} d\rho d\theta \tag{16}$$

the total rate of work dissipation D can be calculated for the ridge mechanism by integrating the expression in Equation (15) over the entire failure surface. Considering that the velocity discontinuity vector in the rotational mechanism is described as $[v] = \omega\rho$ (ω - angular velocity about the axis through point O, and ρ - radial coordinate of the point on the failure

surface) the following expression is derived

$$D = \int_S c[v]\cos\phi dS = 2c\omega \int_{\theta_0^*}^{\theta_h^*} \int_{r_s}^{r^*} \rho^2 \frac{R}{\sqrt{R^2-(\rho-r_c)^2}} d\rho d\theta \tag{17}$$

Introducing the infinitesimal volume element for the ridge mechanism (Figure 2B)

$$dV = \left(\sqrt{R^2-(\rho-r_c)^2} - \frac{b^*}{2}\right)\rho\, d\rho d\theta \tag{18}$$

the total rate of work of gravity forces can be calculated as

$$W_\gamma = \int_V \gamma v\cos\theta dV = \omega\gamma \int_{\theta_0^*}^{\theta_h^*} \int_{r_s}^{r^*} \rho^2 \left[2\sqrt{R^2-(\rho-r_c)^2} - b^*\right]\cos\theta d\rho d\theta \tag{19}$$

where γ is the unit weight of the soil in the slope.

4 | COMPUTATION OF STABILITY ASSESSMENT MEASURES

4.1 | Stability factor

Substituting the work rate expressions in Equations (17) and (19) into Equation (14), the following explicit expression is derived for dimensionless group $\gamma H/c$

$$\frac{\gamma H}{c} = \frac{H\int_{\theta_0^*}^{\theta_h^*}\int_{r_s}^{r*} \rho^2 \frac{2R}{\sqrt{R^2-(\rho-r_c)^2}} d\rho d\theta}{\int_{\theta_0^*}^{\theta_h^*} \cos\theta \int_{r_s}^{r*} \rho^2 \left[2\sqrt{R^2-(\rho-r_c)^2} - b^*\right] d\rho d\theta} \tag{20}$$

with the slope height expressed in the Appendix, Equation (A4). Per definition in Equation (2), the stability factor is the minimum value of the dimensionless group in Equation (20), calculated for independent variable angles θ_0 and θ_h.

As kinematic limit analysis leads to an upper bound to stability factor N_f, a minimization process was carried out with the minimum increment of 0.01° of the two independent variables (θ_0 and θ_h), and the solution was reached when the difference between two consecutive calculations became less than 10^{-6}. In calculations of stability number N_n (reciprocal of the stability factor, Equation (4)), the maximum of N_n was sought.

4.2 | Factor of safety

Because the geometry of the failure mechanism is strongly dependent on internal friction angle ϕ, no explicit expression for the factor of safety could be derived. The reduced shear strength of the soil τ_d (Equation (5)) at which slope failure is impending can be written for the specific case of the Mohr-Coulomb failure criterion as

$$\tau_d = \frac{\tau}{F} = \frac{c}{F} + \sigma_n \frac{\tan\phi}{F} = c_d + \sigma_n \tan\phi_d \tag{21}$$

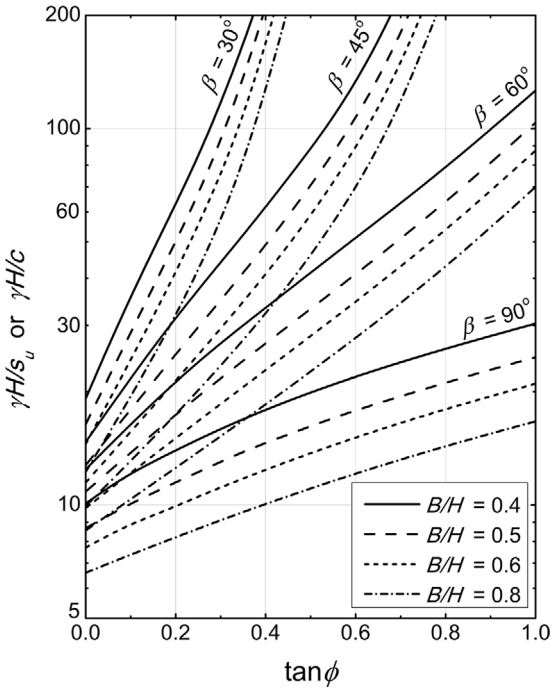

FIGURE 3 Stability factor for narrow slopes as a function of the tangent of the internal friction angle, based on the ridge mechanism (semi-log scale)

Factor of safety F can then be calculated from the following implicit expression

$$F = \frac{c \int_{\theta_0^*}^{\theta_h^*} \int_{r_s}^{r*} \rho^2 \frac{2R}{\sqrt{R^2-(\rho-r_c)^2}} d\rho d\theta}{\gamma \int_{\theta_0^*}^{\theta_h^*} \cos\theta \int_{r_s}^{r*} \rho^2 \left[2\sqrt{R^2-(\rho-r_c)^2} - b^*\right] d\rho d\theta} \tag{22}$$

The expression in Equation (22) is implicit, as both R and r_c are dependent on internal friction angle ϕ (see Equations (6)–(9)), and so is width b^* and the limits of integration. Consequently, angle ϕ (including the limits of integration) in all expressions on the right hand side of Equation (22) need to be replaced with ϕ_d

$$\phi_d = \arctan \frac{\tan\phi}{F} \tag{23}$$

and the equation needs to be solved iteratively with respect to factor of safety F. A minimum of F was sought in an optimization process with a convergence criterion as one used to solve for the stability factor (Section 4.1).

5 | COMPUTATIONAL RESULTS AND DISCUSSION

5.1 | Comparison of computational outcome to existing results

Stability factors calculated for narrow slopes in a B/H range of 0.4 to 0.8, based on the newly constructed ridge mechanism (Figures 1C and 2B), are graphically shown in semi-log scale in Figure 3. Not surprisingly, the stability factor decreases with an increase in the width of the failure mechanism (B/H) and with an increase in the slope inclination angle; the stability factor increases with an increase in the internal friction angle. The numerical outcome of calculations is given in Table 1.

TABLE 1 Stability factor $\gamma H/s_u$ or $\gamma H/c$ for soil slopes based on the ridge failure mechanism

		β (°)				
B/H	***ϕ*** **(°)**	**30**	**45**	**60**	**75**	**90**
0.3	0[a]	23.89	18.01	15.14	13.45	12.35
	15	125.69	53.78	33.63	24.74	20.03
	30	–	79.49	65.31	39.05	28.13
	45	–	–	173.32	67.49	39.84
0.4	0[a]	19.16	14.70	12.44	11.02	9.99
	15	92.50	39.64	25.08	18.65	15.23
	30	–	108.30	48.70	29.57	21.36
	45	–	–	129.70	50.82	30.31
0.5	0[a]	16.39	12.75	10.85	9.59	8.61
	15	73.43	31.46	20.24	15.25	12.51
	30	–	95.35	39.08	24.00	17.39
	45	–	–	103.72	41.24	24.67
0.6	0[a]	14.52	11.47[b]	9.81[b]	8.63[b]	7.70
	15	60.88	26.50	17.36	13.20	10.74
	30	–	79.48	33.01	20.45	14.80
	45	–	–	87.40	35.06	20.99
0.8	0[a]	12.24[b]	9.92[b]	8.55[b]	7.50[b]	6.61[b]
	15	46.07[b]	21.22[b]	14.30[b]	10.94[b]	8.81[b]
	30	–	62.13[b]	26.47[b]	16.53[b]	11.88
	45	–	–	69.96[b]	28.09[b]	16.68

[a]Undrained failure process.

[b]Smooth toe failure surface, all other ridge surfaces.

A comparison of the new results based on the ridge failure mechanism and those for a face mechanism with a smooth failure surface in Park and Michalowski (2018)[6] is shown in Figure 4A. These stability factors are shown for narrow slopes with $B/H \leq 0.8$. The ridge mechanism results are illustrated in blue and those based on the face collapse mechanism with a smooth failure surface[6] are in red. When using the ridge failure mechanism, the largest improvement in the stability factors occurs for vertical slopes, Figure 4B. For practical reasons, the results in Figure 4B are shown for B/H in the range of 0.4 to 0.8, but a wider range is given in Table 2. The improvement of the solution becomes very significant for very steep and narrow slopes. The stability factor calculated based on the "traditional" face failure mechanism overestimates the factor based on the ridge mechanism by nearly 20% (undrained failure of vertical slopes, $B/H = 0.1$). However, the difference becomes insignificant with an increase in the width of the failure mechanism.

Few papers have addressed 3D stability of very narrow slopes. A comparison of stability factors calculated here based on the ridge mechanism and those in Gao et al.[17] is illustrated in Figure 5; the new solution in this paper is marked in blue and Gao et al.[17] in red. For comparison, numerical values of stability factors calculated in this paper and two other papers are given in Table 3 for vertical slopes only. For a vertical slope with $B/H = 0.5$ and for an undrained failure process, the solution of Gao et al.[17] overestimates the ridge mechanism solution by about 29%, while the Park and Michalowski[6] solution overestimates the new outcome in this paper by less than 2%. For a drained failure process in soil with an internal friction angle of 30°, the two other solutions overestimate the solution proposed here by 12.4% and 9.9%, respectively. For a little wider slope ($B/H = 0.8$), the difference between the proposed solution and that in Park and Michalowski[6] becomes insignificant, but the solution of Gao et al.[17] still overestimates the stability factor for an undrained process by 9.4%.

Equally significant is the improvement in accuracy when calculating the factor of safety. Figure 6 graphically indicates the overestimation of factors of safety calculated by Gao et al.[18] and those in this paper using the ridge failure mechanism.

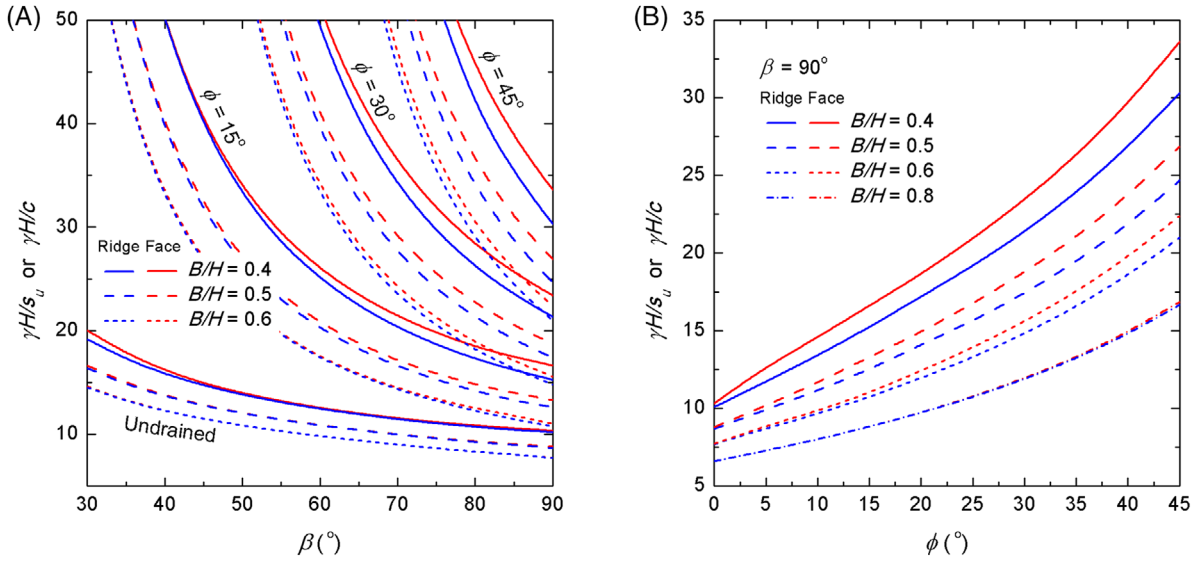

FIGURE 4 Comparison of stability factors for narrow slopes from calculations with the ridge mechanism (blue) and the face failure mechanism (red): (A) comparison as a function of slope inclination angle β, and (B) comparison for vertical slopes as a function of internal friction angle ϕ

TABLE 2 Stability factor $\gamma H/s_u$ or $\gamma H/c$ for vertical slopes

	Undrained failure		$\phi = 45°$	
B/H	**Ridge mechanism[a]**	**Face mechanism[b]**	**Ridge mechanism[a]**	**Face mechanism[b]**
0.1	31.54	37.76	116.24	134.40
0.2	17.14	18.90	58.96	67.20
0.3	12.35	13.08	39.84	44.80
0.4	9.99	10.42	30.31	33.60
0.5	8.61	8.75	24.67	26.88
0.6	7.70	7.81	20.99	22.40
0.7	7.07	7.09	18.46	19.20
0.8	6.61	6.61	16.68	16.86
0.9	6.25	6.25	15.41	15.41
1.0	5.98	5.98	14.49	14.49

[a]Based on the ridge failure mechanism (this study).
[b]Face failure mechanism after Park and Michalowski (2018)[6].

5.2 | Transition from ridge mechanism to a smooth failure surface

Calculations with the ridge mechanism were carried out for below-tow (or deep-seated) failures, but they were either kinematically inadmissible or not critical even for gentle slopes ($\beta = 30°$) confined to narrow widths. However, it is interesting to examine the dependency of the critical mechanism, particularly its depth, on some of the geometrical and material parameters.

Figure 7A illustrates normalized height H^* (or depth) of the critical failure mechanism of a vertical slope as a function of normalized constraint B/H on the width of the mechanism. This figure shows the comparison of the height in the ridge mechanism and the face failure mechanism for an undrained and a drained failures. First, the relationship for the face failure mechanism is linear until the mechanism reaches the toe of the slope ($H^*/H = 1$). This is not surprising given the earlier studies.[6] However, the relationship for the ridge mechanism is nonlinear. In general, for a given constraint B/H the ridge mechanism is deeper and more critical (gives a lower factor of safety). However, there is a threshold B/H when both the ridge and the face mechanism reach the slope toe, and beyond this threshold the best mechanism requires insert b as discussed in Michalowski and Drescher[1] (Figure 2 therein). Both the extracted slice with normalized width b^*/H in

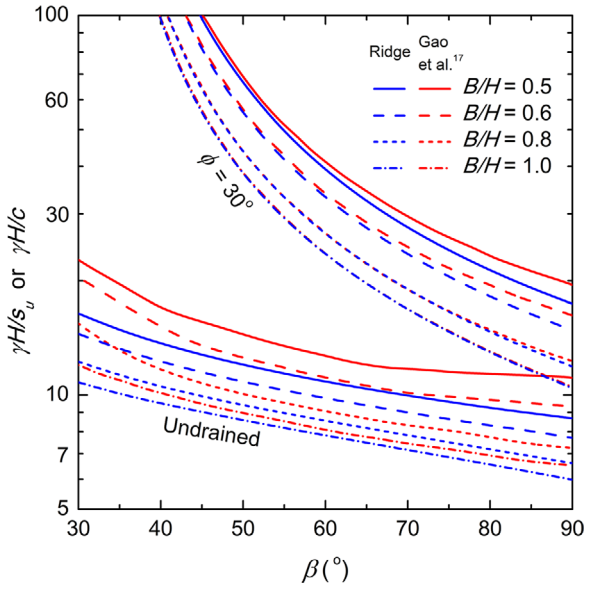

FIGURE 5 Comparison of stability factors based on ridge mechanism (blue) to those in Gao et al.[17] (red)

TABLE 3 Comparison of stability factor $\gamma H/s_u$ or $\gamma H/c$ for vertical slopes

B/H	Source	$\phi = 0°$[a]	$\phi = 15°$	$\phi = 30°$
0.5	Ridge Mechanism (this study)	8.61	12.51	17.39
	Park and Michalowski (2018)[6]	8.75	13.48	18.95
	Gao et al. (2013)[17]	11.10	14.17	19.55
0.6	Ridge Mechanism (this study)	7.70	10.74	14.80
	Park and Michalowski (2018)[6]	7.81	11.19	15.64
	Gao et al. (2013)[17]	9.31	11.79	15.30
0.8	Ridge Mechanism (this study)	6.61	8.81	11.88
	Park and Michalowski (2018)[6]	6.61	8.81	11.93
	Gao et al. (2013)[17]	7.23	9.19	12.26

[a]Undrained failure process.

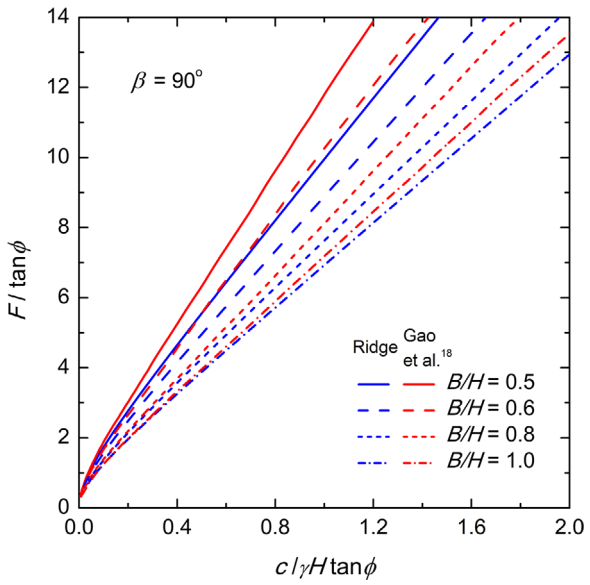

FIGURE 6 Comparison of factors of safety based on ridge mechanism (blue) to those in Gao et al.[18] (red)

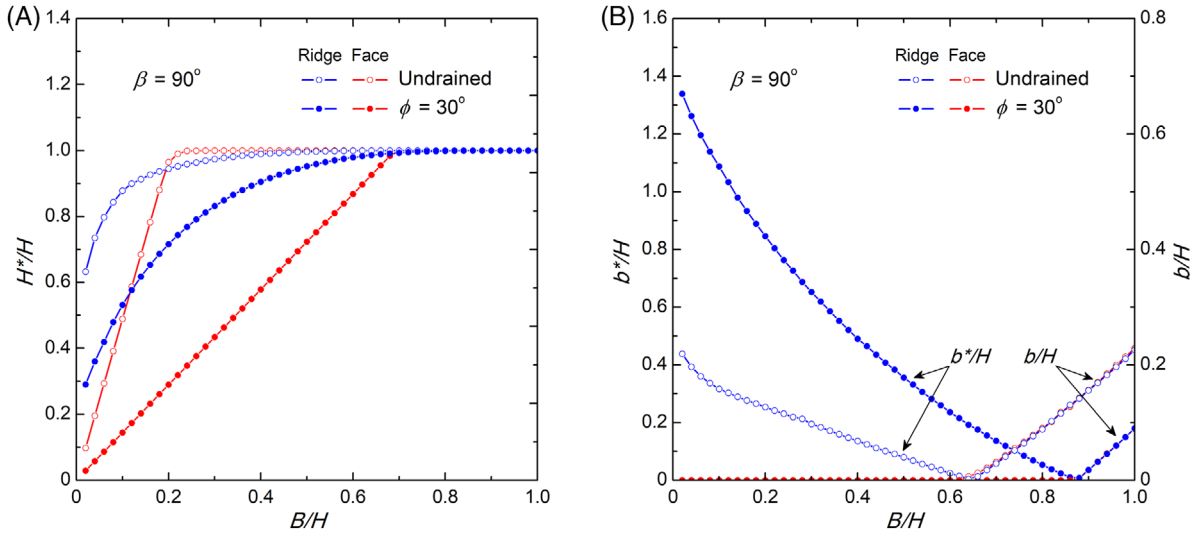

FIGURE 7 Geometric characteristics of a narrow ridge and face failure mechanisms and mechanisms with an insert as functions of width constraint B/H for vertical slopes: (A) normalized height of the critical mechanism H^*/H (see Figure 2b), and (B) normalized width of extracted block b^*/H (see Figure 2b) and normalized width of an insert b/H

the ridge mechanism and the normalized insert width b/H are illustrated in Figure 7B as functions of the width constraint B/H.

First, concentrate on the drained failure (solid blue and red bullets in Figure 7). For a very stringent width constraint of $B/H = 0.2$, the depth of the face mechanism, H^*/H, is less than 0.3 of the slope height (Figure 7A), but for the ridge mechanism, normalized depth H^*/H is more than 0.7. Both the ridge and the face mechanisms reach the toe at the width constraint of about $B/H = 0.7$, but the ridge mechanism still has a small slice of width b^* extracted from it until constraint B/H reaches a value of about 0.88, Figure 7B. For wider slopes ($B/H > 0.88$), the ridge failure surface is no longer critical, and the critical mechanism is one that extends down to the slope toe and includes an insert, as discussed earlier. The increasing width of the insert, b/H, with an increase in B/H is illustrated in the lower right corner of the chart in Figure 7B. The undrained failure (hollow bullets) follows a similar pattern, but a quantitatively different one. It is interesting that the width of a central portion removed from the mechanism, b^*/H, when constructing the ridge failure surface (Figure 2B) is quite large, and the narrower the slope the larger the width of the cut-out b^* (see the left portion of the graph in Figure 7B). The conclusion from this observation is that the critical ridge mechanisms are constructed from quite wide mechanisms with a wide central portion removed, as illustrated in the lower portion of Figure 2B.

The results in Figure 7 were obtained for vertical slopes, but a similar trend was found for slopes with different inclinations. Normalized mechanism depth H^*/H and the width of an insert in critical mechanisms for a 45-degree slope are illustrated in Figure 8A for both the undrained and drained mechanisms. For comparison, the combined results for the vertical slope are replotted in Figure 8B; clearly, the angle of slope inclination has a small influence on the tendency in the geometrical features of the critical mechanism.

Stability factors were calculated for slope inclinations of 30° up to vertical slopes (with 15° intervals), for undrained failures and up to internal friction angle of 45° (with 5° intervals), and selected results were already illustrated in Figures 3 through 5 and in Table 1. For very narrow slopes, B/H of 0.4 and 0.5, all critical mechanisms were ridge mechanisms. However, some of the optimized ridge failure surfaces terminated on the slope face (indicated by $H^*/H < 1$ in Figure 7A) and some reached the toe ($H^*/H = 1$). With an increase of the slope width (B/H) to 0.6, the undrained failures for slopes with inclinations in the range of 45° to 75° had smooth (no ridge) failure surfaces that reached the toe, but the optimized mechanisms for drained failures were still of the ridge type. With a further increase of the slope width to $B/H = 0.8$, only the vertical slopes with internal friction angle $\phi \geq 20°$ remained as the ridge type, whereas the failure surfaces for all other slopes had smooth failure surfaces reaching the slope toe. The same trend was found in calculations of the factor of safety, Figure 6. Not surprisingly, consideration of the ridge mechanism is only important for very narrow slopes.

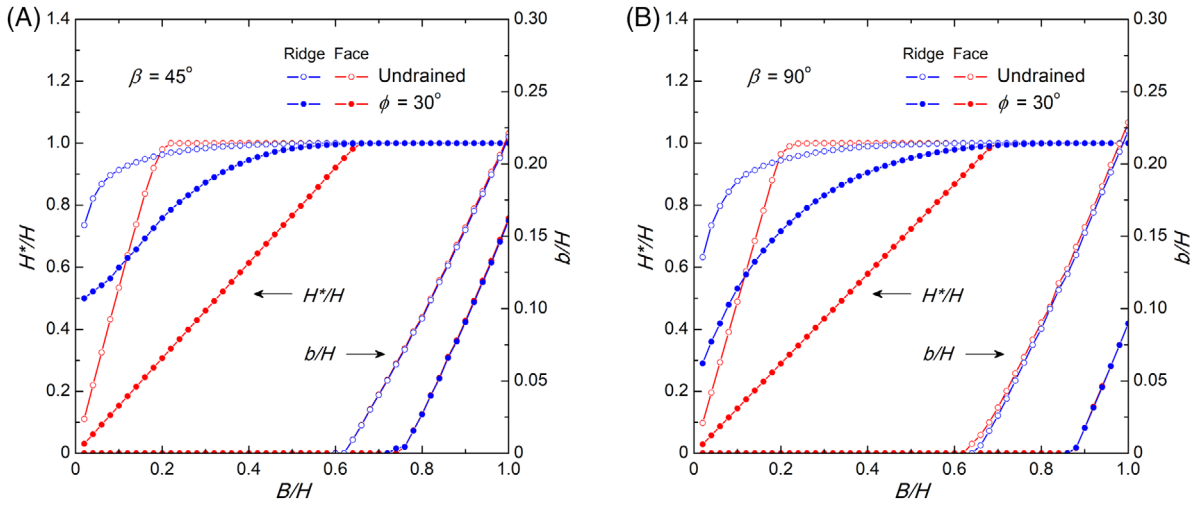

FIGURE 8 Comparison of geometric characteristics of failure mechanisms for 45° slopes and vertical slopes

5.3 | The influence of pore water pressure on stability of narrow slopes

The ridge mechanism appears to be successful in improving the accuracy of safety measures of slopes confined to a narrow width. It is a relatively straightforward process to extend its application to slopes subjected to pore water pressure, as well as to quasi-static seismic forces. First, consider the distribution of the pore water pressure in the slope. In order to find the pore pressure field, the Laplace equation needs to be solved (flow net) for given boundary conditions. In the absence of data defining the boundary conditions, Bishop and Morgenstern[19] suggested an approximate description of the pore pressure field by introducing coefficient r_u varying in a range from 0 to 0.5. This method is adopted here. Once the pore pressure distribution is determined, its influence on stability is calculated by including the work rate of the pore water pressure on the volumetric strain rate of the soil on the right-hand side of inequality (1). It can be proved that this additional term is equivalent to the work of the seepage and buoyancy forces.[20] Because the failure mechanism includes the rigid rotation of one large block, plastic deformation occurs only in the narrow layer of soil on the interface of the rotating block and the stationary material. As this failure zone (thin layer) is considered a surface in the calculations, the appropriate term assumes a simple form

$$W_u = \int_L u[v] \sin\phi dL \tag{24}$$

where u is the pore water pressure, $[v]$ is the velocity discontinuity vector on failure surface L, and ϕ is the internal friction angle.

The results in terms of the stability numbers as defined in Equation (4) are illustrated in Figure 9. While the stability numbers for incompressible (undrained) failures are insensitive to coefficient r_u, the influence of the pore water pressure becomes significant for drained failures, and this influence increases with an increase in the internal friction angle, as illustrated by Figure 9 for coefficient r_u of 0.25 and 0.5. Calculations were performed for slopes with inclinations in the range of 30° to 90°. For narrow slopes ($B/H \leq 0.5$), all failure mechanisms were of the ridge type. With an increase in the slope width, the trend in changing from the ridge mechanism to the smooth toe surface is similar to that for slopes not subjected to pore water pressure, and described in Subsection 5.2.

5.4 | Quasi static seismic load

Including the seismic load in terms of the quasi-static inertial force is a straightforward procedure, where the rate of work of the inertial (seismic) force during incipient failure is calculated[21] and included in inequality (1). In general, this term

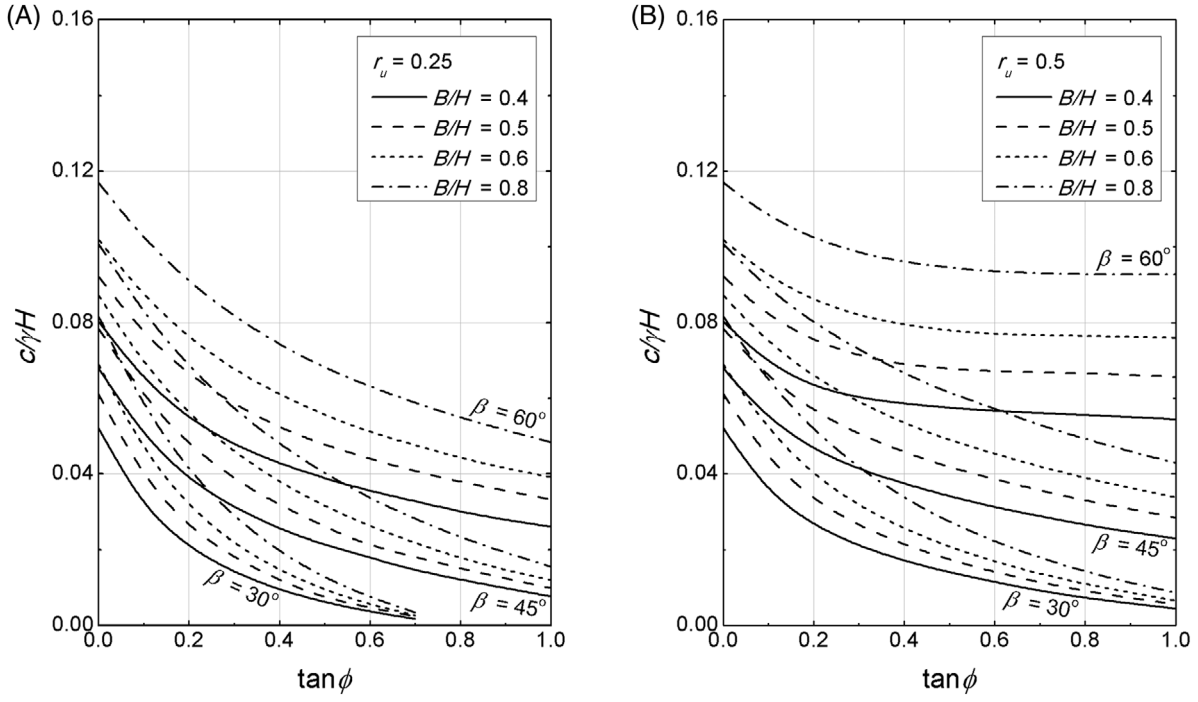

FIGURE 9 Influence of the pore water pressure on stability of narrow slopes: stability number as a function of the tangent of internal friction angle for coefficient $r_u = 0.25$ and $r_u = 0.5$

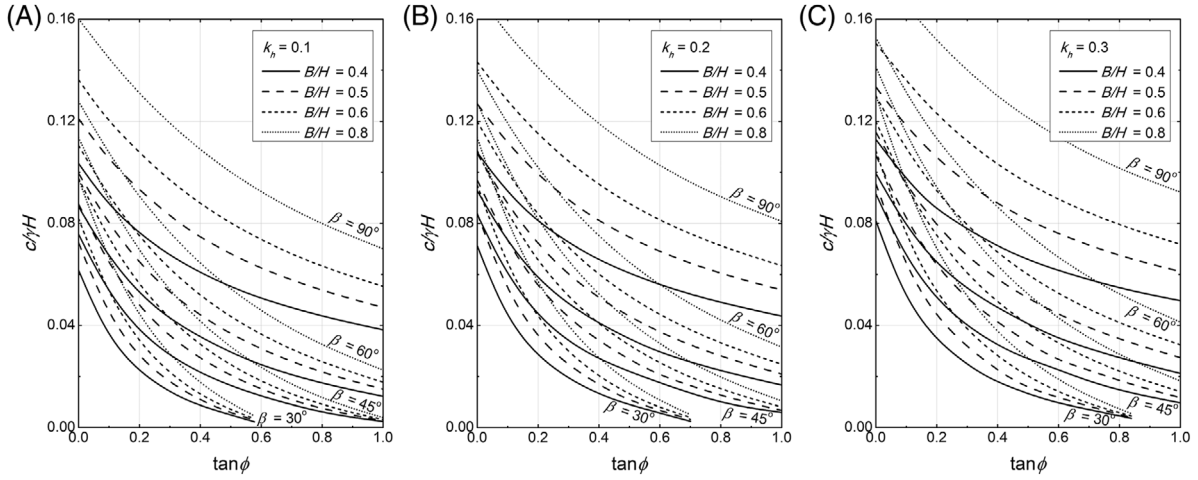

FIGURE 10 Influence of seismic acceleration on stability of narrow slopes: stability number as a function of the tangent of internal friction angle for seismic acceleration coefficient $k_h = 0.1$, $k_h = 0.2$, and $k_h = 0.3$

can be written in terms of the volume integral as

$$W_s = k_h \int_V \gamma v \sin\theta dV \tag{25}$$

where k_h is the coefficient of earthquake acceleration, γ is the soil unit weight, v is the magnitude of the velocity, and θ is the angle between the velocity and the gravity direction (Figure 2). This term was included on the right-hand side of inequality (1), which was used to calculate the rigorous bound to the stability number. The outcome of calculations for seismic acceleration coefficient k_h of 0.1, 0.2, and 0.3 is illustrated in Figure 10. Calculations indicated that the critical

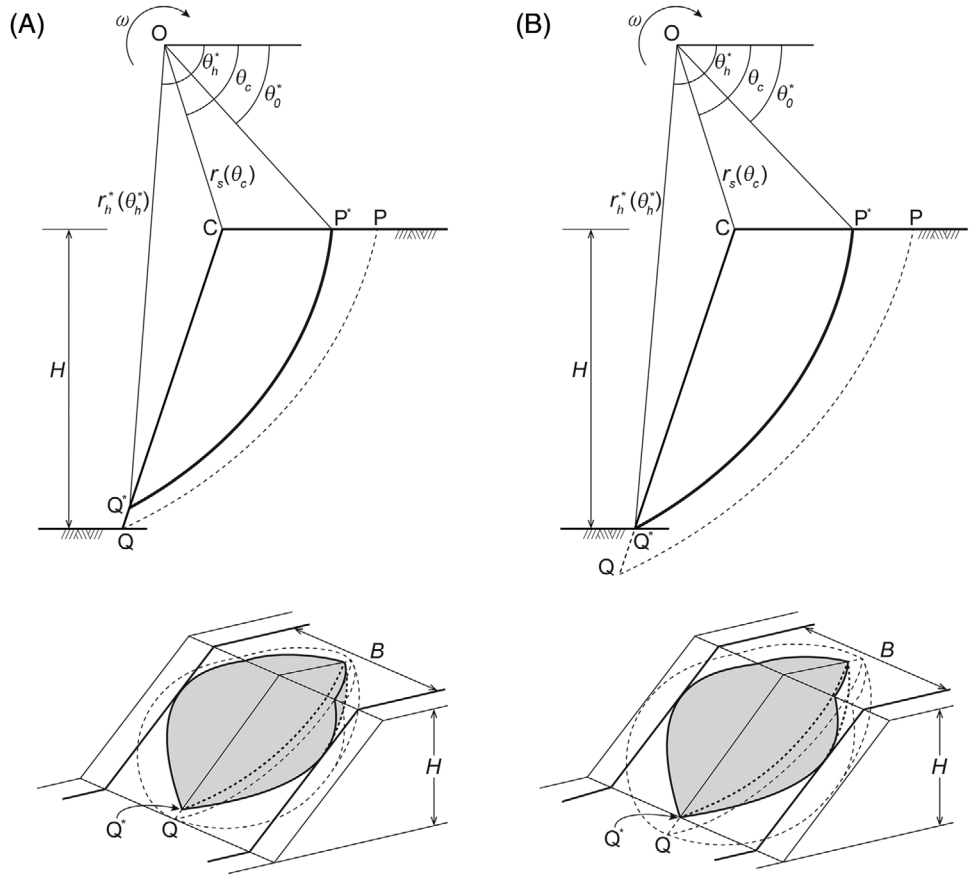

FIGURE 11 Construction of the toe ridge mechanism: (A) cross-section of a ridge mechanism intersecting the slope above the toe, and (B) a toe ridge mechanism

mechanism of failure of narrow slopes subjected to seismic loads is predominantly of the ridge type, particularly for larger seismic accelerations.

5.5 | Ridge-toe mechanism

The optimization process briefly mentioned in Section 4.1 automatically determined whether the critical mechanism (which yields the best bound to a given safety measure) is a ridge mechanism or a mechanism with a smooth failure surface reaching the slope toe. This procedure was also capable of approaching the toe-ridge mechanisms (ridge failure surfaces that reached the slope toe). However, the procedure consistent with the construction of the failure surface as indicated in Figure 2B would always force the optimization process to start searching from a ridge mechanism that does not reach the toe. In order to assure that such a starting point does not lead to a local optimum, a procedure was developed that allowed identifying a toe-ridge mechanism as the first guess in the optimization process. This process is briefly described below.

The mechanism in Figure 11A shows the same ridge failure pattern as in Figure 2B, but with fewer details for clarity. Note that the failure surface illustrated in Figure 2B does not reach the toe. An improvement of the solution to the slope safety measures was attempted by constructing a toe-ridge mechanism. This effort is illustrated in Figure 11B. The toe-ridge mechanism was achieved by selecting an under-toe mechanism such that after removing the vertical slice of width b^* from the rotating block, point Q^* at the bottom of Figure 11B assumes exactly the location on the toe. The procedure for constructing the toe ridge mechanism is elaborate, but the improvement in the stability factor is not significant. For slopes with inclination in the range of 30° to 90° and for both the undrained failure and drained collapse with an internal friction angle up to 45°, the mechanism in Figure 11B provided a better estimate than the mechanism in Figure 2B in

a rather narrow range of parameters, and the difference was found not to exceed 1%. Therefore, all ridge mechanism calculations were carried out with the surface as constructed in Figure 2B.

6 | CONCLUSIONS

The kinematic approach of limit analysis is often used for safety assessment of slopes. When the mechanism of the slope failure is limited to a small width, because of a nearby infrastructure or rock outcrop, the geometric constraint makes it difficult to construct a mechanism that is both kinematically admissible and capable of yielding a good (close to exact solution) upper bound to the stability factor or the factor of safety. A mechanism was constructed with the failure surface that is not smooth, but has a ridge (discontinuous derivative) along the symmetry plane. Calculations indicated that mechanisms suggested earlier in the literature overestimate the newly calculated stability factor based on the ridge mechanism by as much as 29% for vertical narrow slopes ($B/H = 0.5$). The difference becomes smaller with an increase in the slope width, and it becomes almost insignificant when the normalized width of the slope, B/H, increases above 1.0. The newly constructed mechanism was found to accommodate seepage through the slope soil easily and also to account for the seismic load by including the quasi-static force owed to seismic acceleration.

ACKNOWLEDGEMENTS

The work presented in this paper was carried out while the authors were supported by the National Science Foundation, Grant No. CMMI-1901582 and the Horace Rackham School of Graduate Studies at the University of Michigan. The work was also supported by the National Research Foundation of Korea (NRF) grant funded by the Korea government (MSIT), No. 2021R1G1A1003943. This support is greatly appreciated.

DATA AVAILABILITY STATEMENT

The data that support the findings of this study are available from the corresponding author upon reasonable request.

ORCID

Radoslaw L. Michalowski https://orcid.org/0000-0002-9557-4802

REFERENCES

1. Michalowski RL, Drescher A. Three-dimensional stability of slopes and excavations. *Géotechnique*. 2009;59(10):839-850.
2. Michalowski RL. Limit analysis and stability charts for 3D slope failures. *J Geotech Geoenviron Eng*. 2010;136(4):583-593.
3. Michalowski RL. Upper-bound load estimates on square and rectangular footings. *Géotechnique*. 2001;51(9):787-798.
4. Leshchinsky D, Baker R, Silver M. Three dimensional analysis of slope stability. *Int J Numer Anal Meth Geomech*. 1985;9(3):199-223.
5. Zhang F, Leshchinsky D, Baker R, Gao Y, Leshchinsky B. Implications of variationally derived 3D failure mechanism. *Int J Numer Anal Meth Geomech*. 2016;40(18):2514-2531.
6. Park D, Michalowski RL. Intricacies in three-dimensional limit analysis of earth slopes. *Int J Numer Anal Meth Geomech*. 2018;42(17):2109-2129.
7. Drescher A. Limit plasticity approach to piping in bins. *J Appl Mech*. 1983;50(3):549-553.
8. Michalowski RL. Three-dimensional analysis of locally loaded slopes. *Géotechnique*. 1989;39(1):27-38.
9. De Buhan P, Garnier D. Three dimensional bearing capacity analysis of a foundation near a slope. *Soils Found*. 1998;38(3):153-163.
10. Hicks MA, Li Y. Influence of length effect on embankment slope reliability in 3D. *Int J Numer Anal Meth Geomech*. 2018;42(7):891-915.
11. Cremonesi M, Ferri F, Perego U. A basal slip model for Lagrangian finite element simulations of 3D landslides. *Int J Numer Anal Meth Geomech*. 2017;41(1):30-53.
12. Camargo J, Velloso RQ, Vargas EA. Numerical limit analysis of three-dimensional slope stability problems in catchment areas. *Acta Geotech*. 2016;11(6):1369-1383.
13. Tun YW, Llano-Serna MA, Pedroso DM, Scheuermann A. Multimodal reliability analysis of 3D slopes with a genetic algorithm. *Acta Geotech*. 2019;14(1):207-223.
14. Park D, Michalowski RL. Three-dimensional stability assessment of slopes in intact rock governed by the Hoek-Brown failure criterion. *Int J Rock Mech Min Sci*. 2020:104522.
15. Chen W-F. *Limit Analysis and Soil Plasticity*. New York: Elsevier; 1975.
16. Drucker DC, Prager W. Soil mechanics and plastic analysis or limit design. *Q Appl Math*. 1952;10(2):157-165.
17. Gao Y, Zhang F, Lei G, Li D. An extended limit analysis of three-dimensional slope stability. *Géotechnique*. 2013;63(6):518-524.
18. Gao Y, Zhang F, Lei G, Li D, Wu Y, Zhang N. Stability charts for 3D failures of homogeneous slopes. *J Geotech Geoenviron Eng*. 2013;139(9):1528-1538.

19. Bishop AW, Morgenstern N. Stability coefficients for earth slopes. *Géotechnique*. 1960;10(4):129-150.
20. Michalowski RL. Slope stability analysis: a kinematical approach. *Géotechnique*. 1995;45(2):283-293.
21. Nadukuru SS, Michalowski RL. Three-dimensional displacement analysis of slopes subjected to seismic loads. *Can Geotech J*. 2013;50(6):650-661.

How to cite this article: Michalowski RL, Park D. Three-dimensional ridge collapse mechanism for narrow soil slopes. *Int J Numer Anal Methods Geomech*. 2021;45:1972–1987. https://doi.org/10.1002/nag.3251

APPENDIX

Radial coordinate r_s of the slope contour is determined in two distinct regions: PC and CQ (Figure 2A)

$$r_s(\theta) = \begin{cases} r_0 \dfrac{\sin\theta_0}{\sin\theta}, & \text{PC}: \quad \theta_0 < \theta \le \theta_c \\ r_h \dfrac{\sin\theta_h + \cos\theta_h \tan\beta}{\sin\theta + \tan\beta\cos\theta}, & \text{CQ}: \quad \theta_c < \theta \le \theta_h \end{cases} \tag{A1}$$

with angle θ_c calculated from geometric relationships in Figure 2A, and expressed as

$$\theta_c = \arctan \frac{r_h \sin\theta_h - H}{r_h \cos\theta_h + H \cot\beta} \tag{A2}$$

with radius r_h

$$r_h = r_0 e^{(\theta_h - \theta_0)\tan\phi} \tag{A3}$$

and slope height H uniquely related to radius r_0

$$H = r_0 e^{(\theta_h - \theta_0)\tan\phi} \sin\theta_h - r_0 \sin\theta_0. \tag{A4}$$